

# Multi-step *in situ* interface modification method for emission enhancement in semipolar deep-ultraviolet light emitting diodes

LI CHEN,<sup>1,2,†,\*</sup> JIE SUN,<sup>1,†</sup> WEI GUO,<sup>1,2</sup> JASON HOO,<sup>3</sup> WEI LIN,<sup>4</sup> HANGYANG CHEN,<sup>4</sup> HOUQIANG XU,<sup>1,5</sup> LONG YAN,<sup>3</sup> SHIPING GUO,<sup>3</sup> JUNYONG KANG,<sup>4</sup> AND JICHUN YE<sup>1,2,6</sup>

<sup>1</sup>Zhejiang Engineering Research Center for Energy Optoelectronic Materials and Devices, Ningbo Institute of Materials Technology and Engineering, Chinese Academy of Sciences, Ningbo 315201, China

<sup>2</sup>Yongjiang Laboratory, Ningbo 315201, China

<sup>3</sup>Advanced Micro-Fabrication Equipment Inc., Shanghai 201201, China

<sup>4</sup>Department of Physics, Xiamen University, Xiamen 361005, China

<sup>5</sup>University of Chinese Academy of Sciences, Beijing 100049, China

<sup>6</sup>e-mail: jichun.ye@nimte.ac.cn

\*Corresponding author: chenli@nimte.ac.cn

Received 30 March 2022; revised 8 August 2022; accepted 26 September 2022; posted 27 September 2022 (Doc. ID 459897); published 22 November 2022

Semipolar III-nitrides have attracted increasing attention in applications of optoelectronic devices due to the much reduced polarization field. A high-quality semipolar AlN template is the building block of semipolar AlGaIn-based deep-ultraviolet light emitting diodes (DUV LEDs), and thus deserves special attention. In this work, a multi-step *in situ* interface modification technique is developed for the first time, to our knowledge, to achieve high-quality semipolar AlN templates. The stacking faults were efficiently blocked due to the modification of atomic configurations at the related interfaces. Coherently regrown AlGaIn layers were obtained on the *in situ* treated AlN template, and stacking faults were eliminated in the post-grown AlGaIn layers. The strains between AlGaIn layers were relaxed through a dislocation glide in the basal plane and misfit dislocations at the heterointerfaces. In contrast, high-temperature *ex situ* annealing shows great improvement in defect annihilation, yet suffers from severe lattice distortion with strong compressive strain in the AlN template, which is unfavorable to the post-grown AlGaIn layers. The strong enhancement of luminous intensity is achieved in *in situ* treated AlGaIn DUV LEDs. The *in situ* interface modification technique proposed in this work is proven to be an efficient method for the preparation of high-quality semipolar AlN, showing great potential towards the realization of high-efficiency optoelectronic devices. © 2022 Chinese Laser Press

<https://doi.org/10.1364/PRJ.459897>

## 1. INTRODUCTION

AlGaIn-based deep-ultraviolet (DUV) light emitting diodes (LEDs) have wide application prospects in water purification, sterilization, bio-chemical sensing, non-line-of-sight communication, etc. [1]. Although much progress has been made with technological breakthroughs/innovations, the relatively low quantum efficiency of DUV LEDs has always been a major issue to be addressed, putting off the commercialization process of these devices. Besides the strong polarization field in *c*-plane high-Al-content AlGaIn-based DUV LEDs, another key challenge lies in the topmost valence band, which varies from the GaN-like heavy/light hole band to the AlN-like crystal-field split hole band (CH band) [2]. As a result, the emitted light shows TM-dominant polarization behavior with in-plane propagation in traditional *c*-plane DUV LEDs, thus lowering

the light extraction efficiency. Moreover, the first-principles calculations reveal that the radiative transition rate is higher in nonpolar and semipolar multiple quantum wells (MQWs), where the quantum confinement of the topmost CH band is strengthened compared to that of the *c*-plane counterpart [3]. Therefore, nonpolar and semipolar AlGaIn MQWs are the most promising candidates for high-efficiency DUV LEDs.

However, heteroepitaxial semipolar and nonpolar AlN films usually have poor crystal quality, placing restrictions on application in DUV LEDs. Recently, an *ex situ* face-to-face high-temperature annealing (HTA) technique with annealed temperatures up to 1700°C was reported with greatly improved crystalline quality of semipolar AlN [4–7]. After a 3 μm thick AlN film is regrown on the top of the HTA-AlN template, the full width at half maximum (FWHM) of X-ray rocking

curves (XRCs) of the (11 $\bar{2}$ 2) plane can be reduced to as low as 280 arcsec and 294 arcsec along sapphire [0001] and [1 $\bar{2}$ 10] directions, respectively [5]. The low FWHM values of the XRC peaks indicate that the stacking faults have been annihilated efficiently. Despite the remarkable decrease of XRC peak widths, a strongly compressive strain is found in the HTA-AlN layer. This compressive strain is unfavorable to the subsequent growth of AlGa $\bar{N}$  layers due to an enlarged lattice mismatch, which has already been confirmed in *c*-plane AlGa $\bar{N}$  [8]. Furthermore, the energy consuming and time-costing *ex situ* HTA will introduce a large number of point defects such as oxygen, which strongly decreases the optical performance with relatively lower transparency [9]. Lattice bending, twisting, and extra-half planes are also observed in the HTA (11 $\bar{2}$ 2) semipolar AlN, which is a supposed result of the high-temperature thermal treatment [4]. Since the bending lattice deteriorates the post-grown AlN and AlGa $\bar{N}$  layers, an alternative approach to the 1700°C HTA is highly desired.

In this work, a multi-step *in situ* interface modification technique is developed for semipolar AlN films on *m*-plane sapphire. Taking advantage of the surface reconstruction to block the high density of basal plane stacking faults, the residual strains of AlN thin films can be remarkably suppressed due to a relatively low *in situ* treated temperature in a metal–organic vapor phase epitaxy (MOVPE) reactor. The assumed mechanism of hindering the stacking faults is confirmed by transmission electron microscopy. A comprehensive investigation of the distributions and evolution of defects and strains under *in situ* interface modification and *ex situ* HTA is implemented, revealing the huge advantage in crystal quality and optical behavior of post-grown AlGa $\bar{N}$  and DUV LEDs via our multi-step *in situ* interface modification technique. The results presented herein provide a promising strategy towards the suppression of defects and strains and the development of high-quality semipolar solid state light emitters.

## 2. EXPERIMENT

The semipolar AlN template and subsequent DUV LED structures were grown on an *m*-plane sapphire substrate in an AMEC Prismo HiT3 MOVPE reactor. The *in situ* interface modification was conducted under a temperature of 1350°C for half an hour. The NH $_3$  ambiance was used with a reactor pressure of 400 Torr. Reflectivity spectra were monitored *in situ* by BEI OPTICS optical detection. The referenced AlN template by *ex situ* face-to-face HTA was utilized at 1700°C for 3 h in N $_2$  ambiance. Surface morphology was measured by Veeco Dimension 3100 atomic force microscopy (AFM) in tapping mode. Azimuth-dependent XRCs were characterized with Bruker D8 Discover high-resolution X-ray diffraction (HRXRD). The symmetric reciprocal space mapping (RSM) of (11 $\bar{2}$ 2) was measured along both [1 $\bar{1}$ 00] and [11 $\bar{2}$ 3] in-plane directions. The asymmetric RSM was measured through (11 $\bar{2}$ 4) diffraction. The cross-sectional samples for a high-resolution transmission electron microscope (TEM) were prepared by a Helios-G4-CX focused ion beam along (1 $\bar{1}$ 00) and (11 $\bar{2}$ 3) directions and investigated by Talos F200x 200 kV TEM. Annular dark field (ADF) images were acquired for defect and structural analysis. The Renshaw inVia Reflex Raman spectroscope was

utilized for analysis of lattice vibration states in the AlN template. Optical transmission was measured by Perkin-Elmer Lambda 950 UV-VIS spectroscopy. Photoluminescence (PL) measurements were performed using a 193 nm ArF laser as the excitation source, and spectra were collected by a Horiba iHR550 spectrometer.

## 3. RESULTS AND DISCUSSION

The distorted atomic structure of AlN subjected to conventional *ex situ* HTA is demonstrated by both experimental observation and first-principles simulation in Appendix A. A dramatic lattice displacement between as-grown and after 1700°C high-temperature thermal treatment can be observed by high-resolution TEM as shown in Fig. 5 (Appendix A). The atomic movement during the HTA process can be predicted by the molecular dynamic simulations with Vienna Ab initio Simulation Package (VASP) considering the microcanonical ensemble for interpretation. Compared to the ideal AlN structure, a significant atom movement can be observed with a high-temperature treatment, especially in *c* direction. The radial distribution function of N atoms of striped shape along the *c* axis suggests that atom motion in *c* direction is more prominent than in the other directions, resulting in severe lattice bending in the *c* plane. The simulation results are very consistent with the observation of bending lattices in high-resolution TEM images. Due to the disadvantage in distorting atomic lattices, the excessive temperature treating of AlN thin film is discarded in this work, and an alternative approach is herein explored.

In our newly proposed *in situ* interface modification method, the semipolar AlN layer is first grown on the *m*-plane sapphire substrate. Pre-deposition nitridation is introduced to form the uniform (11 $\bar{2}$ 2)-oriented AlN epilayer. A low reactor pressure together with a low V/III ratio under an equilibrium growth condition is chosen to achieve a high growth rate of the (11 $\bar{2}$ 2) plane AlN according to the kinetic Wulff plots [10,11]. Type-I $_1$  basal plane stacking faults with a high density are formed during growth due to the lattice mismatch between semipolar AlN and the sapphire substrate. The energetically favorable type-I $_1$  basal plane stacking faults cannot deform into a glissile partial dislocation, and will penetrate through the crystal without interfaces, grain boundaries, or voids. A high density of stacking faults throughout the epitaxial layers is expected, which will trap the carriers and induce sub-bandgap emission in devices. To avoid the excessive temperature treatment, the intentional introduction of an additional interface to tailor the atomic construction is a good option to block the propagation of stacking faults. The chamber temperature is set to 1350°C, which is slightly higher than the epitaxial temperature to accelerate the surface diffusion and decomposition. According to the calculated phase diagram and absolute surface energy of (11 $\bar{2}$ 2) semipolar AlN, the Al adatom surface construction is most likely to be formed under the Al-rich growing condition [12]. The 2  $\times$  2 surface with 8N-6Al adatoms is more favorable for the AlN (11 $\bar{2}$ 2) surface under N-rich ambiance. Therefore, the NH $_3$  ambiance was adopted to achieve the N-rich condition [12–15]. The incorporation of N atoms will change the formation enthalpies of post-grown AlN, and thus, the films with fewer stacking faults will benefit from this interface

modification. The multi-step *in situ* interface modification procedure proposes three cycles of modified interfaces, each followed by a 1  $\mu\text{m}$  thick high-temperature AlN layer as shown in Fig. 1(a). The *in situ* reflectivity spectrum as a function of time and wafer temperature is shown in Fig. 1(b). The AlN epilayer shows a steady surface reflectivity throughout the *in situ* treated procedure, demonstrating the absence of surface degradation. The mirror-like and crack-free AlN surface with typical semipolar stripe features is obtained in Fig. 1(c).

The surface morphology of *in situ* treated semipolar AlN is investigated by AFM as shown in Fig. 1(d). For comparison purposes, an AFM image of the AlN thin film subject to conventional *ex-situ* thermal annealing is also illustrated. The change of surface features and roughness can be attributed to the different annealing processes. Compared with the *ex situ* annealed AlN, broader stripes with a rough surface are obtained from the *in situ* treated AlN. The root mean square roughness of the *in situ* treated AlN is 2.97 nm, larger than that of the *ex situ* annealed AlN (2.05 nm). The coplanar relationship between the AlN and sapphire substrate is examined by the pole figure as shown in Fig. 1(e). AlN (11 $\bar{2}$ 2) is on-axis, slightly

expanding towards AlN (0002) and sapphire (02 $\bar{2}$ 4) directions. AlN (0002) diffraction with  $\chi = 57.1^\circ$  lies in the direction of  $\phi = 81.2^\circ$ , while sapphire (02 $\bar{2}$ 4) lies in  $\chi = 33.1^\circ$  with  $\phi = 261.2^\circ$ . The opposite in-plane directions of the (0002) peak of AlN and (02 $\bar{2}$ 4) peak of sapphire reveal that the crystalline relationships of AlN and sapphire are  $\langle 11\bar{2}3 \rangle_{\text{AlN}} \parallel \langle 0001 \rangle_{\text{sapphire}}$  and  $\langle 1\bar{1}00 \rangle_{\text{AlN}} \parallel \langle 11\bar{2}0 \rangle_{\text{sapphire}}$ , respectively. The crystal qualities of AlN subject to both *in situ* and *ex situ* treatments were first estimated by the XRCs of (11 $\bar{2}$ 2) diffractions as a function of azimuth angles. The azimuth angle of  $0^\circ$  is defined along the sapphire [0001] direction. As shown in Fig. 1(f), the FWHM values of the XRC peaks of the *in situ* treated AlN template are lower than those of the *ex situ* annealed AlN template, suggesting the lower density of stacking faults in the *in situ* treated AlN layers and consequently less broadening of the (11 $\bar{2}$ 2) diffraction peak. According to the expectation of interface modification by the *in situ* treated technique, the defects are supposed to be blocked at the modified interface. As a result, the defect density decreases gradually from bottom to top AlN layers. Therefore, it can be concluded that the topmost *in situ* treated AlN layer has superior crystal

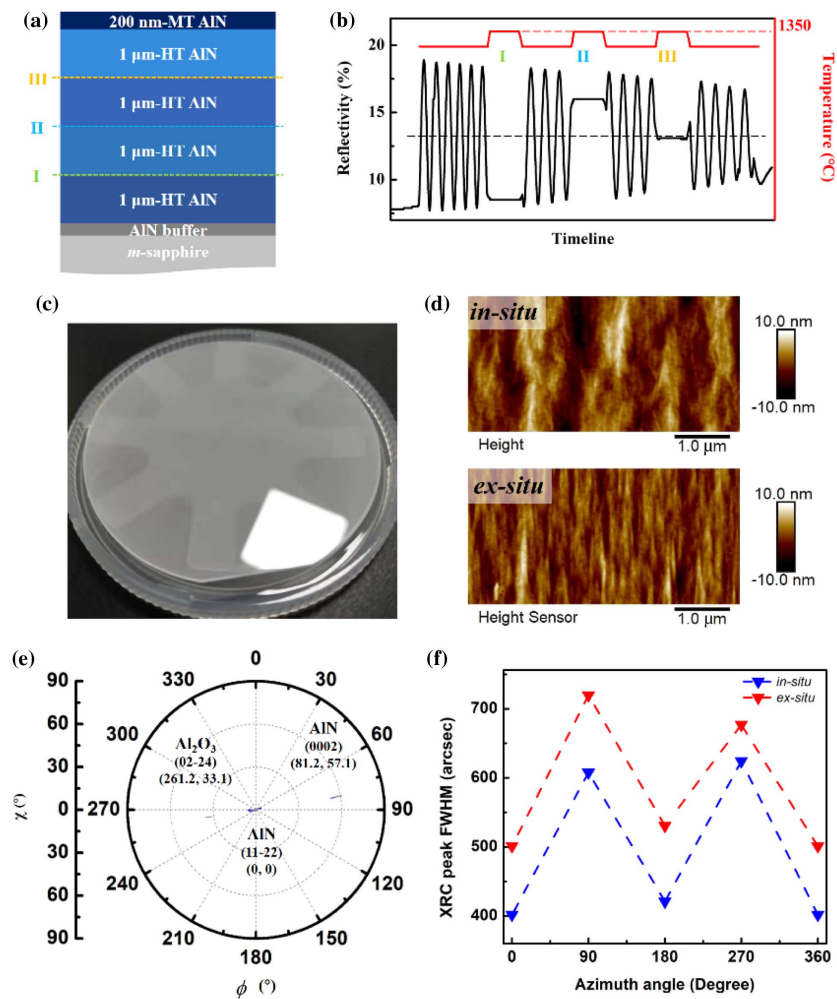


**Fig. 1.** (a) Schematic structure and (b) wafer temperature and the corresponding surface reflectivity of multi-layer *in situ* treated AlN. (c) Mirror-like and crack-free *in situ* treated AlN surface. (d) AFM images of *in situ* and *ex situ* treated AlN. (e) Pole figure of AlN (11 $\bar{2}$ 2), (0002), and sapphire (02 $\bar{2}$ 4) plane diffractions. (f) FWHM of XRC diffraction of AlN templates as a function of azimuth angles.

quality compared to *ex situ* annealed AlN, demonstrating that the multi-step *in situ* interface modification is confirmed as an efficient technique to block the stacking faults. Both *in situ* and *ex situ* treated AlN templates exhibit strong anisotropic distribution of dislocations, which is typical in semipolar III-nitrides due to the existence of basal plane stacking faults [16–18]. The in-plane anisotropy  $\rho$  can be obtained by calculating the relative proportion of the FWHM values of XRCs with an X-ray beam aligned along  $\langle 11\bar{2}3 \rangle$  direction and  $\langle 1\bar{1}00 \rangle$  direction:

$$\rho = \frac{\text{FWHM}_{1\bar{1}00} - \text{FWHM}_{11\bar{2}3}}{\text{FWHM}_{1\bar{1}00} + \text{FWHM}_{11\bar{2}3}}, \quad (1)$$

where  $\text{FWHM}_{1\bar{1}00}$  and  $\text{FWHM}_{11\bar{2}3}$  correspond to the FWHM of XRCs along  $\langle 1\bar{1}00 \rangle$  and  $\langle 11\bar{2}3 \rangle$  directions, respectively.  $\rho = 0.204$  is obtained in the *in situ* treated AlN, which is slightly larger than the value of the *ex situ* annealed AlN ( $\rho = 0.179$ ). Thus, the smaller anisotropy degree of the *ex situ* annealed AlN confirms that the stacking faults are annihilated through bulk recrystallization, while interface modification plays a more dominant role in the case of the *in situ* treatment process, which has less impact on the uniform distribution of defects in the underlying layers.

The extension of stacking faults in the *in situ* treated AlN layer can be observed through ADF images. Considering the anisotropy distribution of dislocations in the semipolar AlN layer, the samples were sliced along both  $\langle 1\bar{1}00 \rangle$  and  $\langle 11\bar{2}3 \rangle$  planes, and ADF images were collected in  $[1\bar{1}00]$  and  $[11\bar{2}3]$  zone axes, respectively. The corresponding diffraction patterns are shown in the inset images of Fig. 2(a). From the ADF images of the AlN layer, a high density of defect lines can be observed in the bottom. These defect lines are basal plane stacking faults of semipolar AlN with an inclined angle of about  $55^\circ$ , most of which disappear beyond the interface of the first *in situ* treatment process. After the second and third modified

interfaces, the density of the defect lines further decreases, leaving behind only several isolated defect lines in the topmost AlN layer. Thus, the proposed *in situ* interface modification is proved to be an efficient way to block stacking faults. The existence of stacking faults in the bottom layer of *in situ* treated AlN presents smaller absorption band edges in Fig. 2(b) than the *ex situ* one due to the slightly narrower bandgaps of stacking faults.

Despite the reduced density of stacking faults, the bulk recrystallization of *ex situ* annealing can result in a distortion of the AlN lattice with strong compressive strain. The Raman shift is shown in Fig. 2(c). Three main first-order vibration modes  $[A_1(\text{TO}), E_2(\text{high}), \text{and } E_1(\text{TO})]$  can be observed in the range of  $550\text{--}750\text{ cm}^{-1}$  as the measurement was taken in  $z(\hat{x}\hat{x})\hat{z}$  geometry on the semipolar AlN surface. The A mode and E mode represent the lattice vibrations along the  $c$  axis and in-plane, respectively. The strain-free position for AlN-like  $E_2(\text{high})$  mode is located at  $656\text{ cm}^{-1}$  [19]. The  $E_2(\text{high})$  peak position of the *in situ* treated AlN shows a slight shift towards a higher wavenumber, suggesting a compressive in-plane strain. The *ex situ* annealed AlN lattice exhibits a significant shift, which can be attributed to the distorted lattice arrangement via recrystallization. Similarly, the  $E_1(\text{TO})$  mode also shifts towards a higher wavenumber for two samples. The  $A_1(\text{TO})$  vibration mode, which represents the strain along the  $c$  axis, also blueshifts towards a higher wavenumber for the *ex situ* annealed AlN film, exhibiting a compressed lattice along the  $c$  axis. The compressed lattice of *ex situ* annealed AlN film is consistent with the result of the bended and twisted lattice reported in our previous work [4]. Conversely, the *in situ* interface modification has little influence on the AlN lattice parameter, as the interface modification instead of bulk recrystallization plays a dominant role in defect blocking. Despite the presence of basal plane stacking faults in the bottom AlN layer, the novel

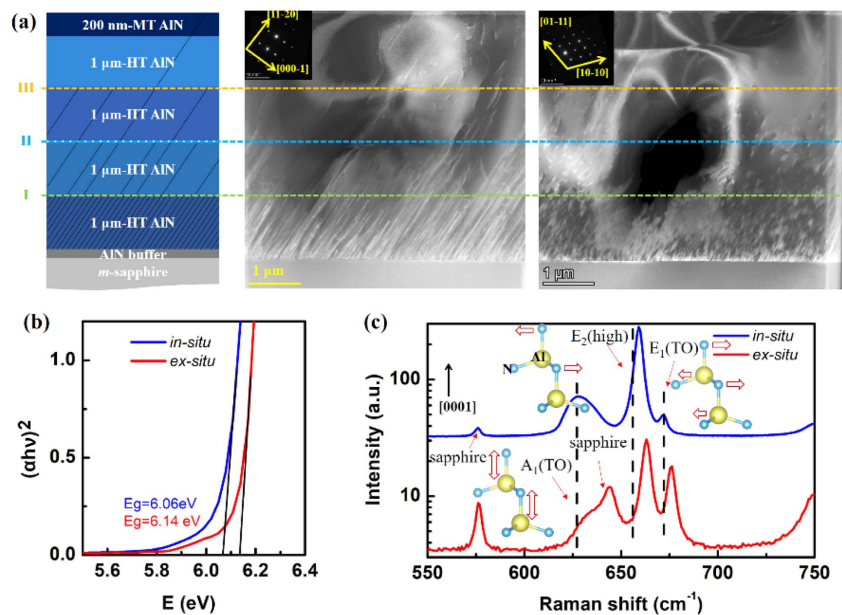


**Fig. 2.** (a) ADF images of *in situ* treated AlN template taken along  $[1\bar{1}00]$  and  $[11\bar{2}3]$  zone axes. (b) Optical transmission spectra and (c) Raman spectra of *in situ* and *ex situ* treated AlN templates.

multi-step *in situ* interface modification technique could lead to better crystal quality and much lower residual strain in the AlN template, revealing itself to be a promising candidate for subsequent AlGaIn epitaxial growth and device fabrications.

The influence of different AlN templates on the subsequent growth of AlGaIn layers and DUV LEDs is further checked. Both *in situ* and *ex situ* treated semipolar AlN templates were reloaded into the MOVPE reactor for the growth of the DUV LED structures. The regrown structure contains a thin AlN regrown layer, AlGaIn strain relaxation layer with Al composition grading from 0.8 to 0.6 at an interval of 10% Al content, n-type  $\text{Al}_{0.6}\text{Ga}_{0.4}\text{N}$ , five pairs of  $\text{Al}_{0.55}\text{Ga}_{0.45}\text{N}/\text{Al}_{0.4}\text{Ga}_{0.6}\text{N}$  MQWs, a 100 nm p-type AlGaIn layer, and a thin GaN cap layer. Figure 3 shows the symmetric and asymmetric

RSM of the DUV LEDs on the different AlN templates. The  $(11\bar{2}2)$  symmetric RSM was measured with an incident X-ray beam aligned along both  $\langle 1\bar{1}00 \rangle$  and  $\langle 11\bar{2}3 \rangle$  directions. As shown in Figs. 3(a) and 3(b), the peaks are misaligned in symmetric RSM along  $\langle 11\bar{2}3 \rangle$  direction, suggesting the tilt of epitaxial film to compensate for the lattice mismatch; no tilt is found in  $\langle 1\bar{1}00 \rangle$  direction. The tilt angles of AlN are determined from RSM along  $11\bar{2}3$  direction to be  $1.79^\circ$  and  $1.10^\circ$  with respect to the sapphire substrate for *in situ* and *ex situ* treated AlN, respectively. A gradually decreased tilt angle can be observed from the bottom to the top of regrown AlGaIn layers. The tilt angles of the n-AlGaIn layers ( $0.66^\circ$  and  $0.59^\circ$  for *in situ* and *ex situ* treated samples, respectively) are very close to each other. This macroscopic tilt of heteroepitaxy

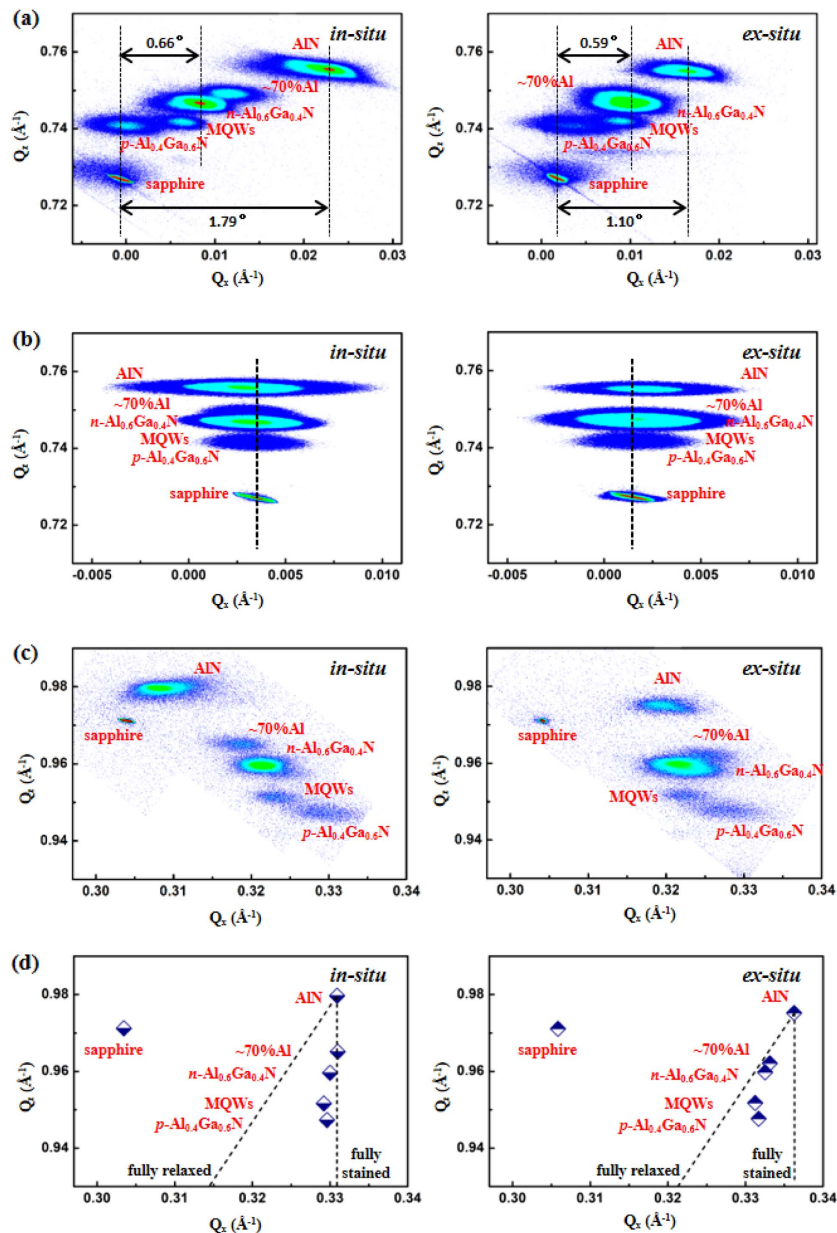


**Fig. 3.**  $(11\bar{2}2)$  symmetric RSM of semipolar DUV LEDs grown on *in situ* and *ex situ* treated AlN templates measured along (a)  $\langle 11\bar{2}3 \rangle$  and (b)  $\langle 1\bar{1}00 \rangle$  directions. (c)  $(11\bar{2}4)$  asymmetric RSM of semipolar DUV LEDs on *in situ* and *ex situ* treated AlN templates. (d) Adjusted  $(11\bar{2}4)$  peak positions of asymmetric RSM according to the different tilt angle of each layer.

thin film is caused by the formation of misfit dislocation arrays with Burgers vector  $\mathbf{b} = 1/3(11\bar{2}0)$  at the heterointerface [20]. It can be confirmed by ADF images, which will be discussed in detail later. The formation of misfit dislocations is a sign of the relaxation process of large shear stresses of an inclined basal plane. Figure 3(c) shows the  $(11\bar{2}4)$  asymmetric RSM; the  $Q_z$  values of the diffraction peaks between two samples are almost identical, suggesting almost the same Al composition of each epilayer. The  $Q_z$  of the *ex situ* annealed AlN template is smaller than that of the *in situ* treated AlN template, consistent with the result of a compressive lattice by Raman spectra. Utilizing the layer tilt angles obtained from the  $(11\bar{2}2)$  symmetric RSM scan, the peak position of each epilayer in  $(11\bar{2}4)$  asymmetric RSM scan is corrected and redrawn in Fig. 3(d). The graded AlGaIn layers on the *in situ* treated AlN template present an almost coherent growth mode, whereas the graded AlGaIn layers are fully relaxed on the *ex situ* annealed AlN template. The relaxation of AlGaIn is always accompanied by defect formation, demonstrated by the significant broadening of the RSM peak of n-AlGaIn in the *ex situ* annealed sample. In contrast, the RSM peak of n-AlGaIn on *in situ* treated AlN is relatively narrow, inheriting the high crystal of the AlN template. After the growth of a thick n-AlGaIn layer, the subsequent MQWs and p-AlGaIn layers show similar properties of two samples.

To illustrate the defect distribution of post-grown AlGaIn layers on *in situ* and *ex situ* treated AlN templates, TEM analysis of two samples sliced along both  $(1\bar{1}00)$  and  $(11\bar{2}3)$  planes was performed. Figures 4(a)–4(d) show ADF images of two samples along  $[1\bar{1}00]$  and  $[11\bar{2}3]$  zone axes. The defect lines in Fig. 4(a) that are inclined at about  $55^\circ$  in the underlying AlN layer can be attributed to type-I<sub>1</sub> basal plane stacking faults. The density of the basal plane stacking faults decreases from the bottom to the top of the *in situ* treated AlN layer as mentioned above. In the post-grown AlGaIn layers, there are still some discontinuous defect lines parallel to the basal plane stacking faults, denoted by DI in the enlarged image in Fig. 4(a). These inclined defect lines in the  $[11\bar{2}3]$  zone axis are isolated short lines different from the typical stacking features of basal plane stacking faults. Accordingly, the defect DI can be attributed to dislocations along the basal plane with Burgers vector components parallel to  $[0001]$ . Thus, the multi-step *in situ* interface modification can efficiently hold back the extension of basal plane stacking faults from the underlying AlN layer. The defect lines denoted by DII were also found in the AlGaIn layer, showing an inclined angle of about  $51^\circ$  with respect to the basal plane, which may originate from the Frank–Shockley partial dislocation with Burgers vector  $\mathbf{b} = 1/6\langle 20\bar{2}3 \rangle$  terminating the basal plane stacking faults.

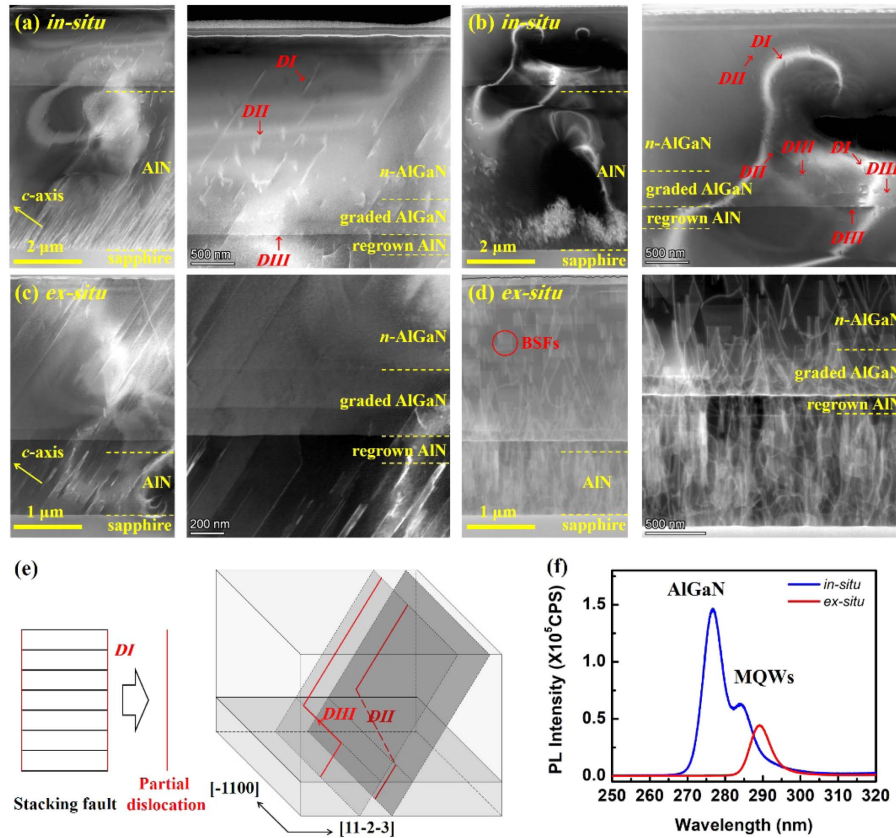


**Fig. 4.** Overall and enlarged ADF images of DUV LEDs on the *in situ* treated AlN template along (a)  $[1\bar{1}00]$  and (b)  $[11\bar{2}3]$  zone axes. ADF images of DUV LEDs on the *ex situ* annealed AlN template and the corresponding enlarged images of defects around the interface along (c)  $[1\bar{1}00]$  and (d)  $[11\bar{2}3]$  zone axes. (e) Schematic of the transformation of three types of defects, DI, DII, and DIII, in AlN and AlGaIn layers. (f) PL spectra of DUV LEDs on different AlN templates.

The existence of defects DI and DII compensates for the strain in AlGaIn layers, thus resulting in the gradual relaxation of strains in RSM. At the heterointerface, there is another form of defect denoted by DIII. Defect DIII at the heterointerface is a misfit dislocation causing the tilt of the thin film as mentioned above. This misfit dislocation distributes at the AlGaIn interfaces with Burgers vector  $\mathbf{b} = 1/3\langle 11\bar{2}0 \rangle$ , which can be hardly found in the ADF image along the  $[1\bar{1}00]$  zone axis since the contrast of a point at the interface is easily overwhelmed by the atomic  $Z$  contrast of different layers. Instead, using ADF images in the  $[11\bar{2}3]$  zone axis, the misfit dislocation lying in the interface of epilayers can be clearly observed as the lateral defect lines marked by red arrows in Fig. 4(b). The formation of defects DIII contributes to the relaxation of shear stresses between AlGaIn layers in the inclined basal plane. In contrast, the *ex situ* annealed sample exhibits completely different defect line features from the *in situ* treated sample. As shown in Figs. 4(c) and 4(d), the inclined defect lines along the basal plane in the AlN layer are greatly reduced in the  $[1\bar{1}00]$  zone axis, but a large number of them still penetrate into the topmost layer, with stacking line features observed in the  $[11\bar{2}3]$  zone axis. The existence of stacking lines in the AlGaIn layer suggests that the basal plane stacking faults are not fully eliminated in the *ex situ* annealed AlN template. From the view of the  $[11\bar{2}3]$  zone axis, the recrystallization of AlN under a high temperature of  $1700^\circ\text{C}$  results in a high density of chaotic defect lines, showing completely different features from the typical DI, DII, and DIII defect features included in Fig. 4(e). There are also lots of extending defects generated from the interface of the regrown AlN and AlGaIn layers, contributing to the relaxation of AlGaIn layers. The high-density defects in the AlGaIn layer on the *ex situ* annealed AlN template have a strong impact on optical behavior. The PL intensities of the two samples are shown in Fig. 4(f), from which the band edge emission peak of the AlGaIn layer can be clearly observed in the *in situ* treated sample, but not in the *ex situ* one. Also, the emission from the MQWs of the *in situ* treated sample is stronger than that of the *ex situ*. The strong enhancement of luminous intensity with much lower defect density achieved in *in situ* treated AlGaIn LEDs shows a great advantage for the realization of high-efficiency optoelectronic devices.

#### 4. CONCLUSION

In this work, a multi-step *in situ* interface modification technique was conducted to achieve high-quality  $(11\bar{2}2)$  semipolar AlN epitaxial thin film by MOVPE. Inspired by the challenges of strain control and the thermal footprint in the thermal annealing treatment of AlN, the proposed *in situ* interface modification technique takes advantage of interface modification by enhancing surface diffusion and reconstruction under N-rich ambiance. As a result, basal plane stacking faults in the semipolar AlN epilayer are efficiently blocked. The FWHMs of XRC peaks in the *in situ* treated AlN templates at all azimuth angles are smaller than in the *ex situ* face-to-face annealed AlN template. Despite the slightly larger in-plane anisotropy of the distributions of the dislocations, the *in situ* treated AlN template shows an almost relaxed strain state compared with the highly compressive strains in the *ex situ* annealed AlN template.

The impact of thermal annealing of the AlN template on subsequent AlGaIn and DUV LED growth is further studied. The superior performance of the *in situ* treated AlN acting as a template for DUV LED is readily interpreted by both structural and optical performances of the devices. The post-grown AlGaIn layers are coherently grown on top of the *in situ* treated AlN, inheriting the higher crystal quality of the AlN template and presenting a strong enhancement in luminous intensity. In contrast, many defects are generated from AlGaIn on *ex situ* annealed AlN, degrading the luminescence intensity of device performance. Overall, the multi-step *in situ* interface modification technique sheds new light on the fabrication of a high-quality semipolar AlN template, providing a promising candidate in the development of high-efficiency optoelectronic devices.

#### APPENDIX A

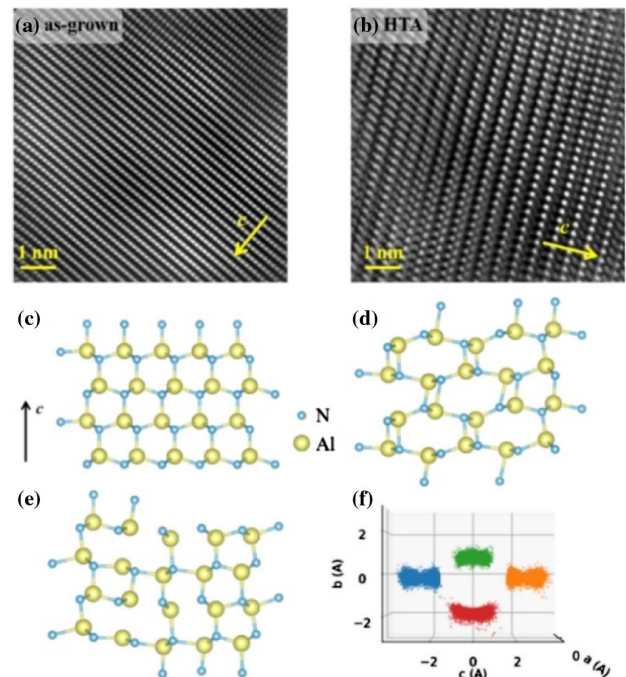


**Fig. 5.** High-resolution TEM images of (a) as-grown and (b) HTA-treated AlN films. (c) Ideal AlN and (d), (e) distorted AlN after high-temperature annealing. (f) Radial distribution function of N atoms around an Al atom by high-temperature annealing.

**Funding.** National Natural Science Foundation of China (61874091, 61974149, 62104233); Key Research and Development Program of Zhejiang Province (2020C01145); Natural Science Foundation of Zhejiang Province (LQ21F40004, LR22F40004); Youth Innovation Promotion Association of the Chinese Academy of Sciences (2020298).

**Disclosures.** The authors declare no conflicts to interest.

**Data Availability.** The data that support the findings of this study are available from the corresponding author upon reasonable request.

<sup>†</sup>These authors contributed equally to this paper.

## REFERENCES

1. M. Kneissl, T. Seong, J. Han, and H. Amano, "The emergence and prospects of deep-ultraviolet light-emitting diode technologies," *Nat. Photonics* **13**, 233–244 (2019).
2. W. Lin, W. Jiang, N. Gao, D. Cai, S. Li, and J. Kang, "Optical isotropization of anisotropic wurtzite Al-rich AlGaN via asymmetric modulation with ultrathin (GaN)<sub>m</sub>/(AlN)<sub>n</sub> superlattices," *Laser Photon. Rev.* **7**, 572–579 (2013).
3. L. Chen, W. Lin, H. Wang, J. Li, and J. Kang, "Reversing abnormal hole localization in high-Al-content AlGaN quantum well to enhance deep ultraviolet emission by regulating the orbital state coupling," *Light Sci. Appl.* **9**, 104 (2020).
4. L. Chen, W. Lin, H. Chen, H. Xu, C. Guo, Z. Liu, J. Yan, J. Sun, H. Liu, J. Wu, W. Guo, J. Kang, and J. Ye, "Annihilation and regeneration of defects in 1122 semipolar AlN via high-temperature annealing and MOVPE regrowth," *Cryst. Growth Des.* **21**, 2911–2919 (2021).
5. M. Jo, Y. Itokazu, S. Kuwaba, and H. Hirayama, "Improved crystal quality of semipolar AlN by employing a thermal annealing technique with MOVPE," *J. Cryst. Growth* **507**, 307–309 (2019).
6. M. Jo, N. Morishita, N. Okada, Y. Itokazu, N. Kamata, K. Tadamoto, and H. Hirayama, "Impact of thermal treatment on the growth of semipolar AlN on *m*-plane sapphire," *AIP Adv.* **8**, 105312 (2018).
7. H. Miyake, C. Lin, K. Tokoro, and K. Hiramatsu, "Preparation of high-quality AlN on sapphire by high-temperature face-to-face annealing," *J. Cryst. Growth* **456**, 155–159 (2016).
8. A. Knauer, A. Mogilatenko, J. Weinrich, S. Hagedorn, S. Walde, T. Kolbe, L. Cancellara, and M. Weyers, "The impact of AlN templates on strain relaxation mechanisms during the MOVPE growth of UVB-LED structures," *Cryst. Res. Technol.* **55**, 1900215 (2020).
9. C. Kai, H. Zang, J. Ben, K. Jiang, Z. Shi, Y. Jia, X. Cao, W. Lu, X. Sun, and D. Li, "Origination and evolution of point defects in AlN film annealed at high temperature," *J. Lumin.* **235**, 118032 (2021).
10. B. Leung, Q. Sun, C. Yerino, and J. Han, "Using the kinetic Wulff plot to design and control nonpolar and semipolar GaN heteroepitaxy," *Semicond. Sci. Technol.* **27**, 024005 (2012).
11. Q. Sun, C. Yerino, B. Leung, J. Han, and M. Coltrin, "Understanding and controlling heteroepitaxy with the kinetic Wulff plot: a case study with GaN," *J. Appl. Phys.* **110**, 053517 (2011).
12. Y. Seta, T. Akiyama, A. Pradipto, K. Nakamura, and T. Ito, "Absolute surface energies of semipolar planes of AlN during metalorganic vapor phase epitaxy growth," *J. Cryst. Growth* **510**, 7–12 (2019).
13. D. Dinh, N. Hu, Y. Honda, and H. Amano, "Pulsed-flow growth of polar, semipolar and nonpolar AlGaIn," *J. Mater. Chem. C* **8**, 8668–8675 (2020).
14. Y. Kangawa, T. Akiyama, T. Ito, K. Shiraishi, and T. Nakayama, "Surface stability and growth kinetics of compound semiconductors: an *ab initio*-based approach," *Materials* **6**, 3309–3360 (2013).
15. Q. Zhuang, W. Lin, W. Yang, W. Yang, C. Huang, J. Li, H. Chen, S. Li, and J. Kang, "Defect suppression in AlN epilayer using hierarchical growth units," *J. Phys. Chem. C* **117**, 14158–14164 (2013).
16. S. Lazarev, S. Bauer, T. Meisch, M. Bauer, I. Tischer, M. Barchuk, K. Thonke, V. Holy, F. Scholz, and T. Baumbach, "Three-dimensional reciprocal space mapping of diffuse scattering for the study of stacking faults in semipolar 1122 GaN layers grown from the sidewall of an *r*-patterned sapphire substrate," *J. Appl. Crystallogr.* **46**, 1425–1433 (2013).
17. D. Dinh, M. Conroy, V. Zubialevich, N. Petkov, J. Holmes, and P. Parbrook, "Single phase 1122 AlN grown on 1010 sapphire by metal-organic vapour phase epitaxy," *J. Cryst. Growth* **414**, 94–99 (2015).
18. J. Stellmach, F. Mehnke, M. Frentrup, C. Reich, J. Schlegel, M. Pristovsek, T. Wernicke, and M. Kneissl, "Structural and optical properties of semipolar 1122 AlGaIn grown on 1010 sapphire by metal-organic vapor phase epitaxy," *J. Cryst. Growth* **367**, 42–47 (2013).
19. U. Habocek, H. Siegle, A. Hoffmann, and C. Thomsen, "Lattice dynamics in GaN and AlN probed with first- and second-order Raman spectroscopy," *Phys. Status Solidi C* **0**, 1710–1731 (2003).
20. A. Romanov, E. Young, F. Wu, A. Tyagi, C. Gallinat, S. Nakamura, S. DenBaars, and J. Speck, "Basal plane misfit dislocations and stress relaxation in III-nitride semipolar heteroepitaxy," *J. Appl. Phys.* **109**, 103522 (2011).